IOP Publishing Measurement Science and Technology
Meas. Sci. Technol. **31** (2020) 064008 (13pp) https://doi.org/10.1088/1361-6501/ab69d5

Assessment of multi-frequency global navigation satellite system precise point positioning models using GPS, BeiDou, GLONASS, Galileo and QZSS

Ke Su[1,2], **Shuanggen Jin**[1,3] **and Guoqiang Jiao**[1,2]

[1] Shanghai Astronomical Observatory, Chinese Academy of Sciences, Shanghai 200030, People's Republic of China
[2] University of Chinese Academy of Sciences, Beijing 100049, People's Republic of China
[3] School of Remote Sensing and Geomatics Engineering, Nanjing University of Information Science and Technology, Nanjing 210044, People's Republic of China

E-mail: sgjin@shao.ac.cn and sg.jin@yahoo.com

Received 29 November 2019, revised 31 December 2019
Accepted for publication 9 January 2020
Published 9 April 2020

Abstract

The development of a global navigation satellite system (GNSS) brings the benefit of positioning, navigation and timing (PNT) services with three or even more available frequency signals. This paper developed five-system multi-frequency precise point positioning (PPP) models based on mathematical and stochastic models. Static positioning performances were evaluated and analyzed with multi-GNSS experiment (MGEX) network datasets and a vehicle-borne kinematic experiment was conducted to verify the kinematic PPP performances. In addition, the receiver clock, zenith tropospheric delay (ZTD), inter-frequency bias (IFB) and differential code bias (DCB) estimates were discussed. Results show that the triple-frequency PPP performances perform slightly better than the dual-frequency solutions, apart from the GPS-related PPP models based on a single ionosphere-free (IF) combined measurement. By introducing the external ionospheric products, the mean convergence time is reduced. For instance, the mean convergence time of ionosphere-constrained (IC) multi-frequency PPP is reduced by 7.4% from 35.7 to 33.1 min and by 19.0% from 7.8 to 6.3 min, for Galileo-only and five-constellation solutions, respectively, compared with dual-frequency IF PPP models. Similarly, the kinematic PPP can also achieve improved performances with more frequency signals and multi-GNSS observations.

Keywords: precise point positioning (PPP), GNSS, triple-frequency, convergence time, positioning accuracy

(Some figures may appear in colour only in the online journal)

1. Introduction

The construction and development of a global navigation satellite system (GNSS) provides users with an opportunity and challenge to operate with multi-frequency signals [1]. The earlier Global Positioning System (GPS) satellites are only capable of transmitting dual-frequency L1 (1575.42 MHz) and L2 (1227.60 MHz) signals. With the modernization of GPS, the new-generation GPS Block IIF satellites can transmit an additional L5 signal (1176.45 MHz) [2]. For the Chinese BeiDou Navigation Satellite System, its development follows a three-step strategy: installation of a demonstration system (BeiDou-1), a regional satellite system (BeiDou-2), and a global satellite system (BeiDou-3) [3]. BeiDou-2 provides users with positioning and navigation services with a constellation of five geostationary-orbit (GEO) satellites,

Table 1. Frequency signals for different GNSS constellations.

GNSS system	Frequency band	Frequency (MHz)
GPS	L1	1575.42
	L2	1227.60
	L5	1176.45
BeiDou-2	B1	1561.098
	B2	1207.14
	B3	1268.52
GLONASS	G1	$1602 + k*9/16, k = -7 \ldots . + 12$
	G2	$1246 + k*716$
	G3	1202.025
Galileo	E1	1575.42
	E5a	1176.45
	E5b	1207.140
	E5	1191.795
	E6	1278.75
QZSS	L1	1575.42
	L2	1227.60
	L5	1176.45
	LEX(6)	1278.45

five inclined-geostationary-orbit (IGSO) satellites and four medium-altitude Earth-orbit (MEO) satellites, which transmits signals on the three bands B1I at 1561.098 MHz, B2I at 1207.14 MHz, and B3I at 1268.52 MHz, respectively [4]. BeiDou-3 has provided global services since 27 December 2018 and consists of five GEO, three IGSO and 27 MEO satellites, capable of broadcasting new signals, namely B1C at 1575.42 MHz, B2a at 1176.45 MHz, and B2b at 1207.14 MHz, respectively [5]. After 2011, some satellites of the Russian Global Navigation Satellite System (GLONASS)-M series and all GLONASS-K satellites have started to transmit code-division multiple access (CDMA) on the G3 signal (1202.025 MHz) [6]. Moreover, the European Galileo system, deployed and developed by the European Commission (EC) and European Space Agency (ESA), provides signals in five frequencies centered at E1 (1575.42 MHz), E5a (1176.45 MHz), E5b (1207.14 MHz), E5 (1191.795 MHz) and E6 (1278.75 MHz) [7]. Quasi-Zenith Satellite System (QZSS), which is the Japanese regional satellite navigation system, provides four frequency signals centered at L1 (1575.42 MHz), L2 (1227.60 MHz), L3 (1176.45 MHz), and LEX (6) (1278.75 MHz) [8]. Table 1 describes each GNSS constellation and the corresponding frequency signals.

The availability of an increasing number of multi-GNSS signal frequencies provides an opportunity to improve carrier phase ambiguity resolution, error source mitigation, cycle slip detection and positioning performances [9–13]. Regarding the ambiguity resolution, some methods exist, such as three-carrier-phase ambiguity resolution (TCAR) and cascading integer resolution (CIR), to improve the ambiguity fix success rate for the relative positioning with triple-frequency signals [14–16]. Geng and Bock [17] proposed a triple-frequency precise-point-positioning (PPP) model and demonstrated its potential to obtain rapid ambiguity resolution. Tegedor and Øvstedal [18] investigated that triple-frequency GPS carrier-phase observations can improve the convergence time of a PPP solution. Guo and Zhang [19] applied triple-frequency BeiDou signals to achieve improved PPP performances compared to dual-frequency ionosphere-free (IF) PPP. Tu *et al* [20] demonstrated that the triple-frequency BeiDou PPP can be applied for precise time transfer with identical accuracy and stability to the dual-frequency IF PPP solution.

Despite the advantages of more signals, some problems also arise, especially for the apparent clock variations [21]. For instance, the precise GPS L1/L2 clock products cannot be directly applied for L5 handling. The inconsistency arises from the time-dependent part of the satellite phase hardware delays in precise satellite estimation (PCE) and is termed as inter-frequency clock bias (IFCB) [22]. The IFCB issue needs to be handled reasonably and is a key problem in multi-frequency data processing. Until now, research focused on multi-frequency multi-GNSS PPP has been limited. Some GNSS satellites can only provide dual-frequency signals at times and it is an important issue to be able to deal with multi-frequency signals properly in the absence of a particular frequency signal.

With this background, this paper contributed to the assessment of multi-frequency PPP models for GPS, BeiDou, GLONASS, Galileo and QZSS. Firstly, we presented the general GNSS observation model and developed four multi-frequency PPP mathematical models as well as their stochastic models. Then, the static positioning performances of GPS-only, BeiDou-only, Galileo-only, GPS/Galileo, GPS/BeiDou/GLONASS/Galileo and GPS/BeiDou/GLONASS/Galileo/QZSS multi-frequency PPP were analyzed compared with dual-frequency IF PPP models. A vehicle-borne kinematic experiment was also used to verify the multi-frequency PPP performances in kinematic scenarios. Finally, some conclusions and perspectives were given.

2. Multi-frequency GNSS PPP models

2.1 General observation model

The linearized equations for GNSS pseudorange and carrier phase observations can be given as [23]

$$p^s_{r,j} = u^s_r \cdot x + dt_r - dt^s + M_w \cdot Z_w + I^s_{r,j} + d_{r,j} - d^s_j + \varepsilon_p \quad (1)$$

$$l^s_{r,j} = u^s_r \cdot x + dt_r - dt^s + M_w \cdot Z_w - I^s_{r,j} + \lambda_j \cdot N^s_{r,j} + b_{r,j} - b^s_j + \varepsilon_\varphi \quad (2)$$

where *s, r* and *j* ($j = 1,2,3$) denote the GNSS satellite, receiver and frequency band, respectively; $p^s_{r,j}$ and $l^s_{r,j}$ are the pseudorange and carrier-phase observed minus computed (OMC) values; u^s_r is the unit vector from the receiver to the satellite; x is the receiver position increment vector; $\mathrm{d}t_\mathrm{r}$ and $\mathrm{d}t_\mathrm{s}$ are the receiver and satellite clock errors; M_w denotes the wet mapping function; Z_w is the zenith wet delay (ZWD); λ_j denotes the *j*th frequency carrier-phase wavelength; and $I^s_{r,j}$ denotes the slant ionospheric delay on the *j*th frequency f^s_j. The

frequency-dependent multiplier factor $\gamma_k^s = (f_1^s/f_k^s)^2, k = 2,3$ can be used to convert the first-order ionospheric delays to different frequencies; $N_{r,j}^s$ denotes the jth frequency integer ambiguity; $d_{r,j}$ and d_j^s denote the receiver and satellite uncalibrated code delays (UCDs), respectively; and $b_{r,j}$ and b_j^s denote the receiver and satellite uncalibrated phase delays (UPDs), respectively. ε_p and ε_φ denote the observation noises of the pseudorange and carrier phase, respectively.

For convenience, we define the following notations in advance:

$$\alpha_{m,n}^s = (f_m^s)^2/[(f_m^s)^2 - (f_n^s)^2], \beta_{m,n}^s = -(f_n^s)^2/[(f_m^s)^2 - (f_n^s)^2] \quad (3)$$

$$\mathrm{DCB}_{m,n}^s = d_m^s - d_n^s, \mathrm{DCB}_{r,m,n} = d_{r,m} - d_{r,n} \quad (4)$$

$$\begin{aligned} p_{r,IF_{m,n}}^s &= \alpha_{m,n}^s \cdot p_{r,m}^s + \beta_{m,n}^s \cdot p_{r,n}^s, l_{r,IF_{m,n}}^s \\ &= \alpha_{m,n}^s \cdot l_{r,m}^s + \beta_{m,n}^s \cdot l_{r,n}^s \end{aligned} \quad (5)$$

$$\begin{aligned} p_{r,IF_{1,2,3}}^s &= e_1 \cdot p_{r,1}^s + e_2 \cdot p_{r,2}^s + e_3 \cdot p_{r,3}^s, l_{r,IF_{1,2,3}}^s \\ &= e_1 \cdot l_{r,1}^s + e_2 \cdot l_{r,2}^s + e_3 \cdot l_{r,3}^s \end{aligned} \quad (6)$$

$$d_{r,IF_{m,n}} = \alpha_{m,n}^s \cdot d_{r,m} + \beta_{m,n}^s \cdot d_{r,n} \quad (7)$$

$$d_{r,IF_{1,2,3}} = e_1 \cdot d_{r,1} + e_2 \cdot d_{r,2} + e_3 \cdot d_{r,3} \quad (8)$$

$$\begin{aligned} b_{IF_{m,n}}^s &= \alpha_{m,n}^s \cdot b_m^s + \beta_{m,n}^s \cdot b_n^s, b_{r,IF_{m,n}} \\ &= \alpha_{m,n}^s \cdot b_{r,m} + \beta_{m,n}^s \cdot b_{r,n} \end{aligned} \quad (9)$$

$$\begin{aligned} b_{IF_{1,2,3}}^s &= e_1 \cdot b_1^s + e_2 \cdot b_2^s + e_3 \cdot b_3^s, b_{r,IF_{1,2,3}} \\ &= e_1 \cdot b_{r,1} + e_2 \cdot b_{r,2} + e_3 \cdot b_{r,3} \end{aligned} \quad (10)$$

where $\alpha_{m,n}^s$, $\beta_{m,n}^s$ represent frequency factors (m, n = 1, 2, 3; $m \neq n$); e_1, e_2 and e_3 denote the coefficients for the triple-frequency PPP model with a single IF combination; and $\mathrm{DCB}_{m,n}^s$ and $\mathrm{DCB}_{r,m,n}$ denote the differential code bias (DCB) for the satellite and receiver, respectively.

To maintain consistency between multi-GNSS observations, we use b1, b2 and b3 to represent observations on three frequencies. In general, the International GNSS Service (IGS) IF satellite clocks generated using the IF observations are consistent with the b1/b2 IF combinations of satellite UCDs [24]. The converted equations for the triple-frequency signals between the b1/b2 IF satellite clocks and uncombined (UC) satellite clocks can be expressed as

$$\begin{cases} dt_1^s = dt_{IF,1,2}^s - \beta_{1,2}^s \cdot \mathrm{DCB}_{1,2}^s \\ dt_2^s = dt_{IF,1,2}^s + \alpha_{1,2}^s \cdot \mathrm{DCB}_{1,2}^s \\ dt_3^s = dt_{IF,1,2}^s - \beta_{1,2}^s \cdot \mathrm{DCB}_{1,2}^s + \mathrm{DCB}_{1,3}^s \end{cases} \quad (11)$$

2.2 Multi-frequency PPP model based on two dual-frequency IF combinations

The triple-frequency measurements can be combined using different dual-frequency IF combinations (i.e. b1/b2, b1/b3, and b2/b3). When the b2/b3 noise amplification is the largest, the b1/b2 and b1/b3 combinations are utilized and we define it as the IF-PPP1 model. When the second or third frequency signal for a GNSS satellite is absent, only one combination is used. After applying the precise satellite orbits and clocks, the linearized equations of the observations transmitting dual-frequency signals equations (12) and (13), and transmitting triple-frequency signals equation (14) can be expressed as [25]

$$\begin{cases} p_{r,IF_{1,2}}^s = u_r^s \cdot x + d\bar{t}_r + M_w \cdot Z_w \\ l_{r,IF_{1,2}}^s = u_r^s \cdot x + d\bar{t}_r + M_w \cdot Z_w + \lambda_1 \cdot \bar{N}_{r,IF_{1,2}}^s \end{cases} \quad (12)$$

$$\begin{cases} p_{r,IF_{1,3}}^s = u_r^s \cdot x + d\bar{t}_r + M_w \cdot Z_w + ifb_{IF1} \\ l_{r,IF_{1,3}}^s = u_r^s \cdot x + d\bar{t}_r + M_w \cdot Z_w + \lambda_1 \cdot \bar{N}_{r,IF_{1,3}}^s \end{cases} \quad (13)$$

$$\begin{cases} p_{r,IF_{1,2}}^s = u_r^s \cdot x + d\bar{t}_r + M_w \cdot Z_w \\ l_{r,IF_{1,2}}^s = u_r^s \cdot x + d\bar{t}_r + M_w \cdot Z_w + \lambda_1 \cdot \bar{N}_{r,IF_{1,2}}^s \\ p_{r,IF_{1,3}}^s = u_r^s \cdot x + d\bar{t}_r + M_w \cdot Z_w + ifb_{IF1} \\ l_{r,IF_{1,3}}^s = u_r^s \cdot x + d\bar{t}_r + M_w \cdot Z_w + \lambda_1 \cdot \bar{N}_{r,IF_{1,3}}^s \end{cases} \quad (14)$$

with

$$\begin{cases} d\bar{t}_r = dt_r + d_{r,IF_{1,2}} \\ ifb_{IF1} = \beta_{1,2}^s \cdot \mathrm{DCB}_{r,IF_{1,2}} - \beta_{1,3}^s \cdot \mathrm{DCB}_{r,IF_{1,3}} \\ \lambda_1 \cdot \bar{N}_{r,IF_{1,k}}^s = \alpha_{1,k}^s \cdot \lambda_1 \cdot N_{r,1}^s + \beta_{1,k}^s \cdot \lambda_k \cdot N_{r,k}^s \\ \qquad + b_{r,IF_{1,k}} - b_{IF_{1,k}}^s - d_{r,IF_{1,2}}. \end{cases} \quad (15)$$

The combined measurements estimate the same receiver clock as the dual-frequency b1/b2 IF PPP and an extra inter-frequency bias (IFB) parameter is necessary to mitigate the receiver UCD inconsistency. Thus, the estimated parameters $E_{IF-PPP1}$ in the IF-PPP1 model include the receiver positions, clock offsets, tropospheric delay, IFB and float ambiguities and can be expressed as

$$E_{IF-PPP1} = [x \quad d\bar{t}_r \quad Z_w \quad ifb_{IF1} \quad \bar{N}_{r,IF_{1,2}}^s \quad \bar{N}_{r,IF_{1,3}}^s]. \quad (16)$$

2.3. Multi-frequency PPP model based on a single IF combination

The measurements for the triple-frequency signals can be grouped into a single observation. With the criteria that they are IF, geometry-free, and have the minimum noises, the combined coefficients e_1, e_2 and e_3 can be determined. The corresponding conditions can be expressed as

$$\begin{cases} e_1 + e_2 + e_3 = 1 \\ e_1 + \gamma_2^s \cdot e_2 + \gamma_3^s \cdot e_3 = 0 \\ (e_1^2 + e_2^2 + e_3^2) = \varepsilon^2 = \min \end{cases} \quad (17)$$

Using the Lagrangian multiplier method to solve the above three conditions, the coefficients can be derived as [26]

$$\begin{cases} e_1 = \dfrac{(\gamma_2^s)^2 + (\gamma_3^s)^2 - \gamma_2^s - \gamma_3^s}{2\cdot[(\gamma_2^s)^2 + (\gamma_3^s)^2 - \gamma_2^s\cdot\gamma_3^s - \gamma_2^s - \gamma_3^s + 1]} \\ e_2 = \dfrac{(\gamma_3^s)^2 - \gamma_2^s\cdot\gamma_3^s - \gamma_2^s + 1}{2\cdot[(\gamma_2^s)^2 + (\gamma_3^s)^2 - \gamma_2^s\cdot\gamma_3^s - \gamma_2^s - \gamma_3^s + 1]} \\ e_3 = \dfrac{(\gamma_2^s)^2 - \gamma_2^s\cdot\gamma_3^s - \gamma_3^s + 1}{2\cdot[(\gamma_2^s)^2 + (\gamma_3^s)^2 - \gamma_2^s\cdot\gamma_3^s - \gamma_2^s - \gamma_3^s + 1]}. \end{cases} \tag{18}$$

In particular, when the second or third frequency of GNSS signal is absent as well, the remaining measurements can be integrated by the dual-frequency IF combination. Then, the linearized equations of the satellites transmitting three frequencies equation (19) and the satellites transmitting signals on two frequencies equation (20) can be written as

$$\begin{cases} p^s_{r,IF_{1,2,3}} = u_r^s\cdot x + d\bar{t}_r + M_w\cdot Z_w \\ l^s_{r,IF_{1,2,3}} = u_r^s\cdot x + d\bar{t}_r + M_w\cdot Z_w + \lambda_1\cdot\bar{N}^s_{r,IF_{1,2,3}} \end{cases} \tag{19}$$

$$\begin{cases} p^s_{r,IF_{1,k}} = u_r^s\cdot x + d\bar{t}_r + M_w\cdot Z_w + ifb_{IF2_{1,k}} \\ l^s_{r,IF_{1,k}} = u_r^s\cdot x + d\bar{t}_r + M_w\cdot Z_w + \lambda_1\cdot\bar{N}^s_{r,IF_{1,k}} \end{cases} \tag{20}$$

with

$$\begin{cases} d\bar{t}_r = dt_r + d_{r,IF_{1,2,3}} \\ \lambda_1\cdot\bar{N}^s_{r,IF_{1,2,3}} = e_1\cdot\lambda_1\cdot N^s_{r,1} + e_2\cdot\lambda_2\cdot N^s_{r,2} + e_3\cdot\lambda_3\cdot N^s_{r,3} \\ \qquad\qquad + b_{r,IF_{1,2,3}} - b^s_{IF_{1,2,3}} - d_{r,IF_{1,2,3}} \\ ifb_{IF2_{1,k}} = d_{r,IF_{1,k}} - d_{r,IF_{1,2,3}} \\ \lambda_1\cdot\bar{N}^s_{r,IF_{1,k}} = \alpha^s_{1,k}\cdot\lambda_1\cdot N^s_{r,1} + \beta^s_{1,k}\cdot\lambda_k\cdot N^s_{r,k} \\ \qquad\qquad + b_{r,IF_{1,k}} - b^s_{IF_{1,k}} - d_{r,IF_{1,2,3}}. \end{cases} \tag{21}$$

Noteworthily, the estimable IFB parameters in the IF-PPP2 model do not need to be considered when all processing satellites can transmit signals on three frequencies. Hence, the estimated parameters $E_{IF-PPP2}$ in the IF-PPP2 model include the receiver positions, clock offsets, tropospheric delay, optional IFB and float ambiguities, and are expressed as

$$E_{IF-PPP2} = [x \quad d\bar{t}_r \quad Z_w \quad (ifb_{IF2_{1,k}}) \quad \bar{N}^s_{r,IF_{1,2}} \quad \bar{N}^s_{r,IF_{1,3}}]. \tag{22}$$

2.4. Multi-frequency UC PPP model

The multi-frequency UC PPP model, known as UC-PPP, employs raw satellite observations, in which it also works when a frequency signal is absent. The linearized equations of the UC-PPP model can be written as

$$\begin{cases} p^s_{r,1} = u_r^s\cdot x + d\bar{t}_r + M_w\cdot Z_w + \bar{I}^s_{r,1} \\ l^s_{r,1} = u_r^s\cdot x + d\bar{t}_r + M_w\cdot Z_w - \bar{I}^s_{r,1} + \lambda_1\cdot\bar{N}^s_{r,1} \\ p^s_{r,2} = u_r^s\cdot x + d\bar{t}_r + M_w\cdot Z_w + \gamma_2^s\cdot\bar{I}^s_{r,1} \\ l^s_{r,2} = u_r^s\cdot x + d\bar{t}_r + M_w\cdot Z_w - \gamma_2^s\cdot\bar{I}^s_{r,1} + \lambda_2\cdot\bar{N}^s_{r,2} \\ p^s_{r,3} = u_r^s\cdot x + d\bar{t}_r + M_w\cdot Z_w + ifb_{UC} + \gamma_3^s\cdot\bar{I}^s_{r,1} \\ l^s_{r,3} = u_r^s\cdot x + d\bar{t}_r + M_w\cdot Z_w - \gamma_3^s\cdot\bar{I}^s_{r,1} + \lambda_3\cdot\bar{N}^s_{r,3} \end{cases} \tag{23}$$

with

$$\begin{cases} d\bar{t}_r = dt_r + d_{r,IF_{1,2}} \\ \bar{I}^s_{r,1} = I^s_{r,1} + \beta^s_{1,2}\cdot \mathrm{DCB}_{r,1,2} \\ ifb_{UC} = \beta^s_{1,2}/\beta^s_{1,3}\cdot \mathrm{DCB}_{r,1,2} - \mathrm{DCB}_{r,1,3} \\ \lambda_1\cdot\bar{N}^s_{r,1} = \lambda_1\cdot N^s_{r,1} + b_{r,1} - b^s_1 + (\beta^s_{1,2} - \alpha^s_{1,2})\cdot d_{r,1} \\ \qquad\qquad - 2\cdot\beta^s_{1,2}\cdot d_{r,2} \\ \lambda_2\cdot\bar{N}^s_{r,2} = \lambda_2\cdot N^s_{r,2} + b_{r,2} - b^s_2 - 2\cdot\alpha^s_{1,2}\cdot d_{r,1} \\ \qquad\qquad + (\alpha^s_{1,2} - \beta^s_{1,2})\cdot d_{r,2} \\ \lambda_3\cdot\bar{N}^s_{r,3} = \lambda_3\cdot N^s_{r,3} + b_{r,3} - b^s_3 + (\gamma_3^s\cdot\beta^s_{1,2} - \alpha^s_{1,2})\cdot d_{r,1} \\ \qquad\qquad - (\beta^s_{1,2} + \gamma_3^s\cdot\beta^s_{1,2})\cdot d_{r,2}. \end{cases} \tag{24}$$

The estimated parameters E_{UC-PPP} in the UC-PPP model include the receiver positions, clock offsets, tropospheric delay, IFB, slant ionospheric delays and float ambiguities, and can be expressed as

$$E_{UC-PPP} = [x \quad d\bar{t}_r \quad Z_w \quad ifb_{UC} \quad \bar{I}^s_{r,1} \quad \bar{N}^s_{r,1} \quad \bar{N}^s_{r,2} \quad \bar{N}^s_{r,3}]. \tag{25}$$

2.5. Multi-frequency ionosphere-constrained PPP model

The multi-frequency ionosphere-constrained (IC) PPP model, namely IC-PPP, adds virtual observations and their corresponding constraints for the ionospheric parameters. Similarly, it is flexible enough to deal with the available observations for the dual- or triple-frequency signals. The linearized observation equations of the IC-PPP model can be written as

$$\begin{cases} p^s_{r,1} = u_r^s\cdot x + d\bar{t}_r + M_w\cdot Z_w + \beta^s_{1,2}\cdot \mathrm{DCB}_{r,1,2} + I^s_{r,1} \\ l^s_{r,1} = u_r^s\cdot x + d\bar{t}_r + M_w\cdot Z_w - I^s_{r,1} + \lambda_1\cdot\bar{N}^s_{r,1} \\ p^s_{r,2} = u_r^s\cdot x + d\bar{t}_r + M_w\cdot Z_w - \alpha^s_{1,2}\cdot \mathrm{DCB}_{r,1,2} + \gamma_2^s\cdot I^s_{r,1} \\ l^s_{r,2} = u_r^s\cdot x + d\bar{t}_r + M_w\cdot Z_w - \gamma_2^s\cdot I^s_{r,1} + \lambda_2\cdot\bar{N}^s_{r,2} \\ p^s_{r,3} = u_r^s\cdot x + d\bar{t}_r + M_w\cdot Z_w + \gamma_3^s\cdot\beta^s_{1,2}\cdot \mathrm{DCB}_{r,1,2} + ifb_{UC} \\ \qquad + \gamma_3^s\cdot I^s_{r,1} \\ l^s_{r,3} = u_r^s\cdot x + d\bar{t}_r + M_w\cdot Z_w - \gamma_3^s\cdot I^s_{r,1} + \lambda_3\cdot\bar{N}^s_{r,3} \\ \tilde{I}^s_{r,1} = I^s_{r,1} \end{cases} \tag{26}$$

with

$$\begin{cases} d\bar{t}_r = dt_r + d_{r,IF_{1,2}} \\ ifb_{UC} = \beta^s_{1,2}/\beta^s_{1,3}\cdot \mathrm{DCB}_{r,1,2} - \mathrm{DCB}_{r,1,3} \\ \lambda_k\cdot\bar{N}^s_{r,k} = \lambda_k\cdot N^s_{r,k} + b_{r,k} - b^s_k - d_{r,IF_{1,2}} \end{cases} \tag{27}$$

where $\tilde{I}^s_{r,1}$ can be derived from an external ionospheric product, such as a global ionosphere map (GIM). The estimated parameters $E_{Ion-PPP}$ in the IC-PPP model include the receiver positions, clock offsets, tropospheric delay, DCB, IFB, slant ionospheric delays and float ambiguities, and can be expressed as

$$E_{Ion-PPP} = [x \quad d\bar{t}_r \quad Z_w \quad \mathrm{DCB}_{r,1,2} \quad ifb_{UC} \quad I^s_{r,1} \quad \bar{N}^s_{r,1} \quad \bar{N}^s_{r,2} \quad \bar{N}^s_{r,3}]. \tag{28}$$

Table 2. Characteristics of multi-frequency PPP models for different GNSS constellations.

Models	GNSS constellations	Signal combination	e_1	e_2	e_3	Noise amplification
IF-PPP1	GPS/QZSS	L1-L2	2.546	−1.546	0.000	2.978
	GPS/QZSS	L1-L5	2.261	0.000	−1.261	2.588
	BeiDou-2	B1-B2	2.487	−1.487	0.000	2.898
	BeiDou-2	B1-B3	2.944	0.000	−1.944	3.527
	Galileo	E1-E5a	2.261	−1.261	0.000	2.588
	Galileo	E1-E5b	2.422	0.000	−1.422	2.809
IF-PPP2	GPS/QZSS	L1-L2-L5	2.327	−0.360	−0.967	2.546
	BeiDou-2	B1-B2-B3	2.566	−1.229	−0.338	2.865
	Galileo	E1-E5a-E5b	2.315	−0.836	−0.479	2.507
UC-PPP/IC-PPP	GPS/BeiDou-2/Galileo/QZSS	b1	1.000	0.000	0.000	1.000
		b2	0.000	1.000	0.000	1.000
		b3	0.000	0.000	1.000	1.000

2.6. Stochastic models

The satellite elevation weighting method in PPP models can be applied with a sine mapping function. Assuming that the uncorrelated observations share the same prior noise, the variance—covariance of the UC observations can be written as [27, 28]

$$\sum\nolimits_{UC-PPP} = \delta_0^2 \cdot I \tag{29}$$

where $\delta_0 = a/\sin(E)$, a is usually set to be 0.2–4.0 m for pseudorange and 0.002–0.004 m for carrier-phase observations [29]. The variances of the different GNSS observations can refer to the literature [30]. E denotes the satellite elevation; I denotes the identity matrix. Then, the stochastic models for other PPP schemes can be obtained by the error propagation law, which can be expressed as

$$\begin{cases} \sum_{IF1_{1,2,3}} = \delta_0^2 \cdot \begin{bmatrix} (\alpha_{1,2}^s)^2 + (\beta_{1,2}^s)^2 & \alpha_{1,2}^s \cdot a_{1,3}^s \\ \alpha_{1,2}^s \cdot a_{1,3}^s & (\alpha_{1,3}^s)^2 + (\beta_{1,3}^s)^2 \end{bmatrix} \\ \sum_{IF1_{1,k}} = \delta_0^2 \cdot [(\alpha_{1,k}^s)^2 + (\beta_{1,k}^s)^2] \\ \sum_{IF1_{1,2,3}} = \delta_0^2 \cdot [(e_1)^2 + (e_2)^2 + (e_3)^2] \\ \sum_{IF2_{1,k}} = \delta_0^2 \cdot [(\alpha_{1,k}^s)^2 + (\beta_{1,k}^s)^2]. \end{cases} \tag{30}$$

The external ionospheric observation variances can be determined with a time-varying function, the weight method of which is written as [30]:

$$\sigma^2 = (1 + 0.2\Delta t) \cdot \sigma_{ion}^2 \cdot mf(z)^2 \tag{31}$$

with

$$mf(z) = \left[1 - \sin^2 z/(1 + H_{ion}/R)^2\right]^{-1/2} \tag{32}$$

$$\sigma_{ion}^2 = \begin{cases} \sigma_{ion,0}^2, & t < 8 \text{ or } t > 20 \text{ or } B > \pi/3 \\ \sigma_{ion,0}^2 + \sigma_{ion,1}^2 \cos(E) \cos(\frac{t-14}{12}\pi), & \text{other} \end{cases} \tag{33}$$

where Δt represents the number of epochs. σ_{ion}^2 denotes the spatial variance. H_{ion} denotes the ionosphere single-layer height. R denotes the average Earth radius. t denotes the local time at the ionospheric pierce point (IPP). The variance $\sigma_{ion,0}^2$ and $\sigma_{ion,1}^2$ are both set to 0.09 m^2.

Table 2 summarizes the characteristics of multi-frequency PPP models for GPS, BeiDou, Galileo and QZSS, including the models, GNSS constellations, signal combination, combined coefficients and noise amplification factors. The characteristics of the GLONASS solutions are not shown here because the signals have different frequency numbers due to the application of the frequency-division multiple access (FDMA) technique. We can observe that IF-based noise amplifications range from 2.5 to 3.5 and the combination in the IF-PPP2 model shows the smallest noise amplification.

3. Data processing and performance analysis

3.1. Data processing strategy

To evaluate the performances of the proposed multi-frequency PPP models, datasets of 18 stations from the multi-GNSS experiment (MGEX) network for September 1–30, 2018 (day of year (DOY) from 244 to 273) were selected and utilized for numerical analysis. Figure 1 shows the geographic distribution of the selected 18 MGEX stations. To show the ionospheric conditions, the geomagnetic K_{p} index values for September 1–30, 2018 are shown in figure 2. All stations can receive quad-system observations from the GPS, BeiDou, GLONASS and Galileo constellations. In addition, the stations in the Asia-Pacific area can also track QZSS signals. These stations were performed for GPS-only, BeiDou-only, Galileo-only, GPS/Galileo, GPS/BeiDou/GLONASS/Galileo and GPS/BeiDou/GLONASS/Galileo/QZSS multi-frequency PPP schemes in static modes. Moreover, a set of vehicle-borne kinematic data was utilized to verify the multi-frequency PPP performances in kinematic scenarios.

Table 3 summarizes the detailed processing strategies for multi-frequency PPP. Precise orbit and clock offset products

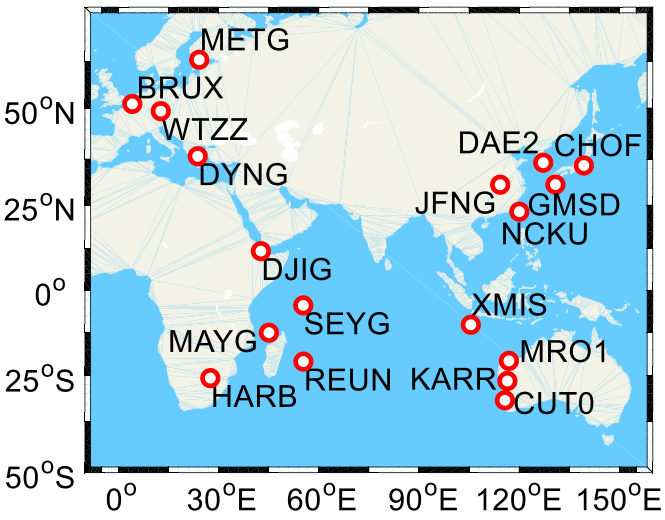

Figure 1. Geographical distribution of the selected MGEX stations.

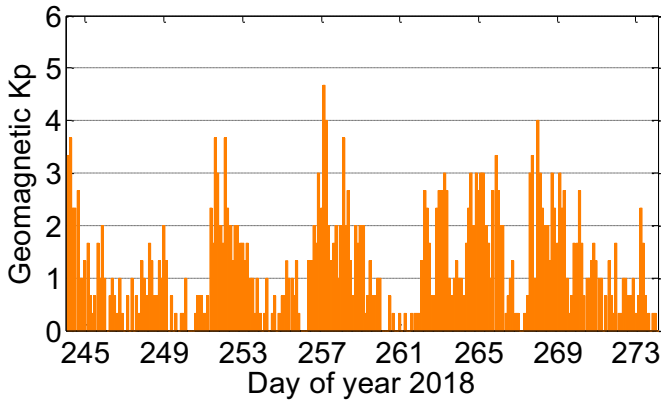

Figure 2. Geomagnetic K_p index in September 2018.

at intervals of 5 min and 30 s, respectively, provided by Deutsches GeoForschungsZentrum (GFZ), are adopted [31]. The satellite DCB values are corrected by the MGEX values [32]. A set of satellite and receiver antenna calibrations, namely igs14.atx, are utilized. Asthe third frequency phase center correction is unavailable now, the corresponding corrections adopt the same values as for the second frequency [33]. In Kalman filtering of PPP processing, the ZWD is estimated as a random-walk process and the receiver clock is estimated as white noise. When integrated multi-GNSS combined positioning is carried out, the intersystem bias (ISB) parameters are needed for the newly added GNSS systems and are estimated as constants. For multi-frequency IC-PPP schemes, the receiver DCB at the receiver ends is estimated as constant to separate the absolute slant ionospheric delay values. The satellite UCDs contain time-invariant and time-varying parts. The time-invariant parts of the UCDs are absorbed by the estimated float ambiguities. The receiver IFBs are estimated as constants or absorbed by receiver clock biases to compensate for the time-invariant parts of the UCDs on the third frequency. The existing time-dependent parts of the UCDs will cause phase anomaly and influence the performance of the multi-frequency PPP. The marginal IFCB variations can be neglected for the BeiDou satellite [22], Galileo satellites [1] and QZSS satellites [34]. The time-dependent UCDs of GPS satellites will cause systematic errors of several centimeters when the estimated ambiguities are sufficiently accurate and it is not appropriate to ignore the GPS time-dependent UCDs. Considering the official GPS satellite IFCBs products have not been released, we assigned stochastic properties to the float ambiguities so that they can absorb the time-dependent parts of the UCDs. Based on the characteristics of the four multi-frequency PPP models, the ambiguities for the GPS IF-PPP1 L1/L5, UC- and IC-PPP L5 signals are estimated as random-walk process with spectral density values of 3×10^{-5} m^2 s^{-1}, and the spectral density values of the estimable GPS IF-PPP2 L1/L2/L5 ambiguities are set to 3×10^{-7} m^2 s^{-1} [35].

3.2. Static PPP performances

Taking the stations MRO1 and KARR on September 5, 2018 (DOY 248) as examples, figure 3 depicts the positioning errors of these stations in the north (N), east (E) and up (U) components among the different multi-frequency PPP schemes for GPS, BeiDou, Galileo, GPS/Galileo, GPS/BeiDou/GLONASS/Galileo and five-constellation solutions, together with the observed satellite numbers and position dilution of precision (PDOP) values. The error values are shifted by the same account to avoid overlapping (the same operation as in figures 4 and 5). The RMS of positioning errors for different PPP schemes are also shown in the figure, calculated from the convergence epoch to the end epoch. The convergence criterion is defined when the component of the error is less than 0.1 m and remains within 0.1 m in the subsequent epochs. Comparing the BeiDou and Galileo triple-frequency PPP results, the IF-PPP1, IF-PPP2 and UC-PPP solutions generally agree with each other. It is reasonable that the three PPP models are equivalent because their weight matrices are transformed according to the law of covariance propagation [40]. For GPS-only PPP, the performances of the three PPP models emerge differently due to the impact of the time-variant UCDs, which cannot be fully absorbed by the corresponding assigned float ambiguities. Because the existing combined ambiguities are all assigned stochastic properties, the performance of GPS under IF-PPP2 is seriously deteriorated, compared with the IF-PPP0 solution. With upgrading and development of the GPS IFCB products, the problem can effectively be resolved [21]. By comparing the GPS and BDS PPP results, we can see that the BeiDou positioning accuracy is worse than that of the GPS. The reason for this is that the accuracy of BeiDou satellite orbits is worse than that of GPS, and the BeiDou constellation has a poorer geometry. As the BeiDou-3 satellites have officially provided global services since December 27, 2018, we can expect BeiDou to achieve better results. For the IC-PPP model, it leads to different results since *a priori* information is added on the ionosphere parameters. In addition, compared with single-constellation PPP solutions, multi-GNSS PPP is more stable and has less noise for the increasing number of visible satellites, and thus better spatial distribution.

Table 3. Data-processing strategies for multi-frequency multi-GNSS PPP.

Items	Strategies
Involved solutions	b1/b2 IF PPP (IF-PPP0); IF-PPP1; IF-PPP2; UC-PPP; IC-PPP
Data span	September 1–30, 2018
Signal selection	GPS/QZSS: L1/L2/L5; BeiDou-2: B1/B2/B3; GLONASS: G1/G2; Galileo: E1/E5a/E5b
Estimator	Kalman filter
Sampling rate	MGEX static datasets: 30 s; Vehicle-borne kinematic data: 1 s
Elevation cutoff	7°
Satellite orbit and clock	Fixed by MGEX orbit and clock products
Satellite DCB	Corrected using MGEX DCB products for PPP [32]
Tropospheric delay	Modified Hopfield for dry part and estimated for wet part as random-walk process (10^{-9} m^2 s^{-1}) [36]
Ionospheric delay	IF-PPP0/IF-PPP1/IF-PPP2: eliminated by IF combinations; UC-PPP/IC-PPP: estimated as white-noise process (1×10^4 m^2)
Relativistic effect	General relativistic models [37]
Sagnac effect	Corrected model [38]
Phase windup effect	Corrected model [39]
Satellite and receiver antenna	Corrected with the values from MGEX and IGS [38]
Tide displacement	Corrected, including solid Earth, pole and ocean tide [37]
Station reference coordinates	IGS SINEX solutions
Receiver coordinate	Static PPP: estimated as constants; Kinematic PPP: estimated as white noise process (1×10^5 m^2).
Receiver clock	Estimated as white-noise process (1×10^5 m^2)
Receiver ISB	Estimated as constants
Receiver IFB	Estimated as constants or absorbed by receiver clocks
Receiver DCB	Estimated as constants or absorbed by receiver clocks
Phase ambiguities	GPS IF-PPP1 L1/L5, UC- and IC-PPP L5 ambiguities: estimated as random-walk process (3×10^{-5} m^2 s^{-1}); GPS IF-PPP2 L1/L2/L5 ambiguities: (3×10^{-7} m^2 s^{-1}); Other ambiguities: estimated as constants.

Figure 4 shows the raw clock time series of stations MRO1 and KARR for different PPP models. As depicted, the estimated receiver clock has the same variation for different PPP models. The results also confirm that the estimated receiver clocks of IF-PPP0, IF-PPP1, UC-PPP and IC-PPP are referred to the b1/b2 IF clock ($\bar{dt_r} = dt_r + d_{r,IF_{1,2}}$), and the estimable receiver clock of IF-PPP2 is the combined effect of the clock and receiver hardware delays ($\bar{dt_r} = dt_r + d_{r,IF_{1,2,3}}$). These variations of the estimated clock are mainly caused by the changes of the satellite clocks. The receiver clock time series of the two stations emerge similarly but they have a system bias that is related to the hardware delay.

For the multi-frequency PPP models, the troposphere delay parameters are estimated as a random-walk process. Figure 5 shows the comparison of the estimated zenith troposphere delay (ZTD) of stations MRO1 and KARR for different PPP models. The RMS of troposphere errors for different PPP schemes are also shown in the figure. The troposphere zenith path delay (ZPD) products with a sampling rate of 5 min are utilized as reference values, which have a typical formal error of 1.5–5 mm [41]. Apart from the GPS under the IF-PPP2 model, no significant difference (maximal accuracy difference of 1 mm) was found in the accuracy of the estimated troposphere delay. The reasons for the anomaly have been discussed above.

As discussed before, the estimated receiver clock absorbs the hardware delay in the IF-PPP2 model and the IFB parameters have to be considered in other triple-frequency PPP models. Figure 6 shows the comparison of IFB estimates of stations MRO1 and KARR of the IF-PPP1, UC-PPP and IC-PPP models for GPS, BeiDou, Galileo and QZSS in five-constellation PPP solutions. The IFB time series of the two stations have the same variations. These biases are very stable except for the GPS cases. According to equations (15), (24) and (27), we can clearly see that the estimable IFBs of UC-PPP and IC-PPP refer to the same values. The equations can confirm the relationships of the estimable values between the IF-PPP1 and UC-PPP (IC-PPP) models. The ratio of the estimated ifb_{IF1} and ifb_{UC} is $\beta^s_{m,n}$, which is -1.261 for GPS/QZSS, -1.944 for BeiDou-2, and -1.422 for Galileo. To verify our estimable values, the receiver DCBs ($\mathrm{DCB}_{r,1,2}$ and $\mathrm{DCB}_{r,1,3}$) extracted from MGEX were utilized to calculate the corresponding IFB values according to the corresponding equations and also listed in figure 6. These values are very close to the estimated IFB values and can further confirm our derivation of the estimable IFB parameters.

For the multi-frequency IC-PPP model, the receiver b1/b2 DCB is estimated to separate the pure ionospheric observations and then virtual ionospheric observations can be added. Figure 7 shows the comparison of receiver DCB estimates of stations MRO1 and KARR of the IC-PPP model in the five-constellation solution. The corresponding receiver b1/b2 DCB values extracted from MGEX provided by CAS are also listed. For GPS, BeiDou and Galileo, the estimated DCB time series were found to be very stable for the whole day. For the station MRO1, a systematic deviation was found throughout the

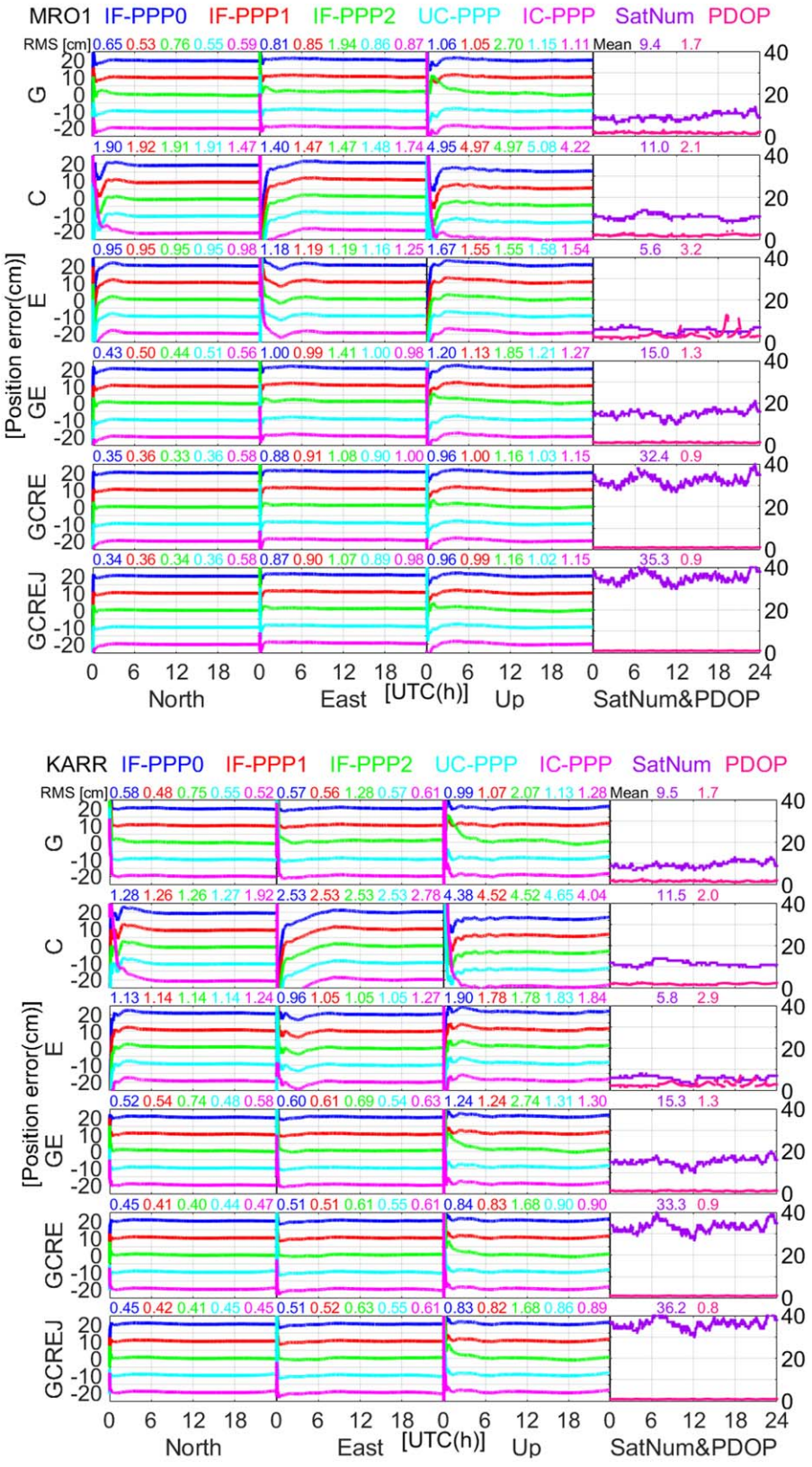

Figure 3. Comparison of the positioning error between different PPP models for GPS, BeiDou, Galileo, GPS/Galileo, GPS/BeiDou/GLONASS/Galileo and five-constellation solutions at stations MRO1 and KARR (DOY 248/2018, $K_p \approx 2.17$). The corresponding satellite numbers and PDOP values are also shown. The abbreviations G, C, R, E and J denote GPS, BeiDou, GLONASS, Galileo and QZSS, respectively.

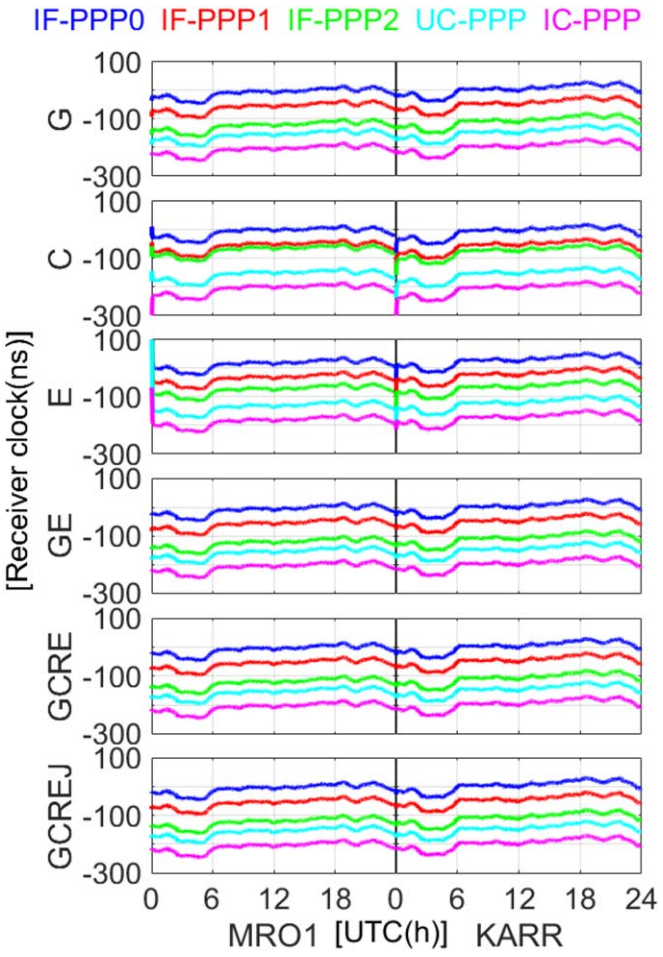

Figure 4. Receiver clocks of stations MRO1 and KARR (DOY 248/2018) between different PPP models for GPS, BeiDou, Galileo, GPS/Galileo, GPS/BeiDou/GLONASS/Galileo and five-constellation solutions.

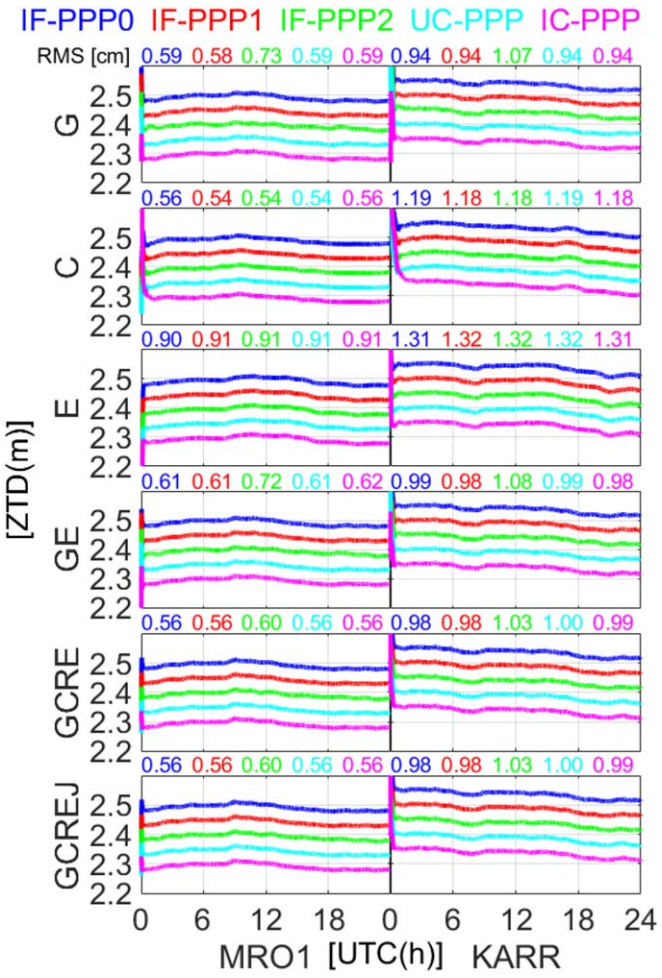

Figure 5. Estimated ZTD of stations MRO1 and KARR between different PPP models for GPS, BeiDou, Galileo, GPS/Galileo, GPS/BeiDou/GLONASS/Galileo and five-constellation solutions.

whole day (approximately 1.0 ns), which may be caused by the strong correlation between the ionosphere delay and DCB. It also indicates that the estimated receiver DCB will absorb part of the ionospheric delay errors.

Figure 8 shows the mean convergence time of 18 stations by different PPP models with different schemes. Table 4 summarizes the root mean square (RMS) errors of the multi-frequency PPP models in multi-constellation combinations. We can see that the BeiDou-only and Galileo-only PPP clearly perform worse than the GPS-only solution, and the integration of the multi-GNSS can significantly improve the multi-frequency PPP performances in terms of convergence time and positioning accuracy. Apart from the GPS under the IF-PPP2 model, the solutions of triple-frequency PPP agree well with each other in general and the triple-frequency PPP models show slightly better performances than the dual-frequency solution in terms of convergence time and positioning accuracy. By introducing the GIM products, the mean convergence time of the multi-frequency PPP model is further reduced. For instance, compared with the IF-PPP0 models, the mean convergence time of the IC-PPP is reduced by 7.4% from 35.7 to 33.1 min and by 19.0% from 7.8 to 6.3 min for the Galileo-only and five-constellation IC-PPP, respectively. Owing to the growing weighting for virtual ionospheric observation in the filter process, a small but not obvious improvement can be seen in the positioning accuracy with the ionosphere constraint.

3.3. *Vehicle-borne kinematic PPP tests*

For kinematic PPP test purposes, approximately 2 h of vehicle-borne GPS/BeiDou/GLONASS/Galileo/QZSS data were collected in Beijing, China on March 2018 and reprocessed from 09:50 to 12:00 Coordinated Universal Time (UTC). The data have a sampling rate of 1 Hz and are collected from the vehicle-borne three-dimensional mobile surveying system. The system is equipped with a five-system NovAtel GPSCard receiver and inertial measurement unit of SPAN LCI type. The same type of receiver was also set up in the Beijing Foreign Studies University as a base station to perform a relative positioning solution through GNSS/INS tight coupled resolution of Inertial Explorer 8.60 software, the results of which were regarded as an external reference to assess kinematic PPP performances [42]. The trajectory of the experiment is shown in figure 9.

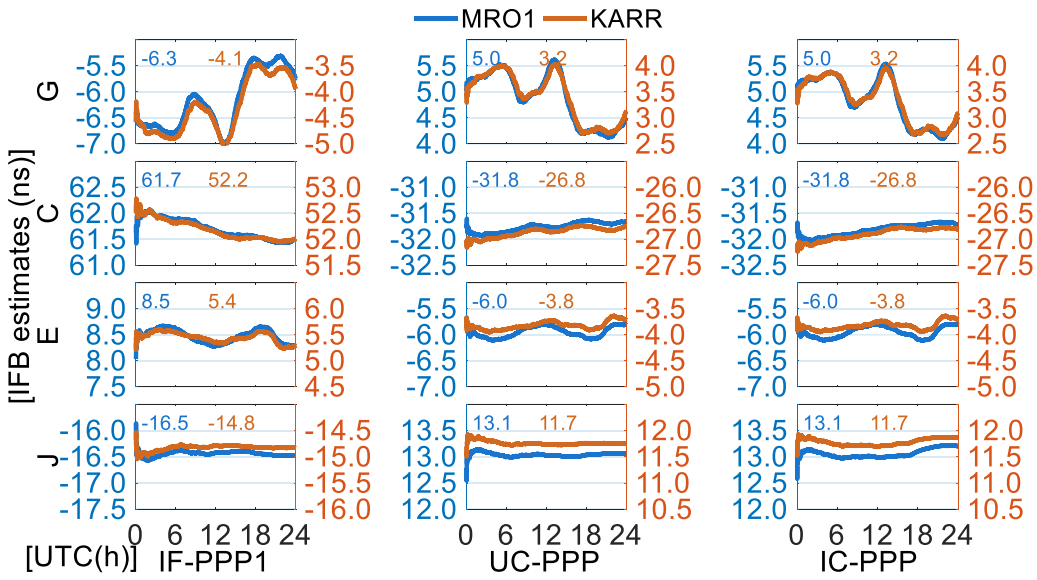

Figure 6. Time series of IFB estimates of stations MRO1 and KARR of the IF-PPP1, UC-PPP and IC-PPP models for GPS, BeiDou, Galileo and QZSS in five-constellation multi-frequency PPP solutions.

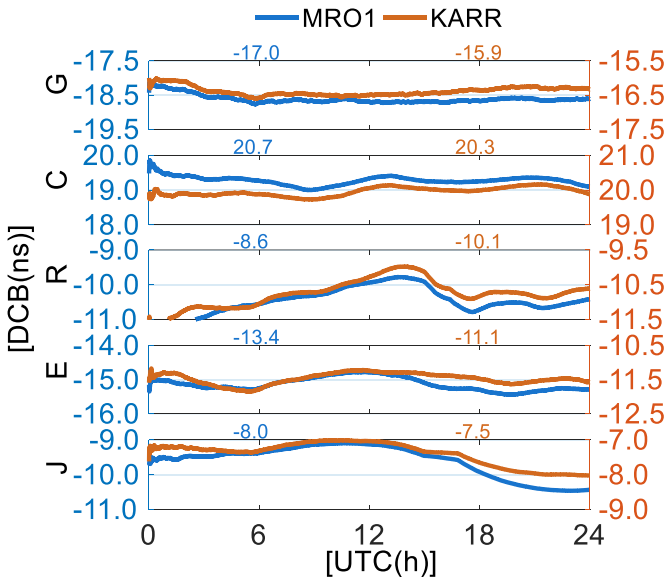

Figure 7. Time series of receiver DCB estimates of stations MRO1 and KARR of the IC-PPP model for five-constellation solutions.

Using this kinematic dataset, the GPS, BeiDou, and GPS/BeiDou/GLONASS/Galileo/QZSS dual- and triple-frequency PPP were performed. Figure 10 depicts the satellite visibility and corresponding PDOP values for the GPS-only, BeiDou-only and five-constellation PPP solutions. The mean number of observed satellites for GPS, BeiDou and five-constellation are 9.8, 7.9 and 29.2, respectively, and the mean corresponding PDOP values are 2.0, 4.0 and 0.9, respectively. We can observe that multi-GNSS integration can significantly increase the observed number of satellites and improve their visual condition. Figure 10 shows the positioning errors of the dual- and triple- frequency PPP models for the GPS, BeiDou and five-constellation solutions compared with the reference results. In addition, the RMS of the kinematic PPP positioning errors based on the last 60 min is given in the figure, in which the PPP solutions have converged. As we can see in figure 11, the BeiDou dual-frequency PPP performs worse than the GPS dual-frequency solution, particularly in the U direction. It is not surprising that thiscan be attributed to satellite spatial distribution, which can be seen in figure 10. Comparing the different BeiDou-only PPP results, we find that the triple-frequency PPP performs better than the dual-frequency solution, which is particularly pronounced for the IC-PPP solution. As for the GPS-based PPP, they all agree well with the reference results and the triple-frequency solutions run more stably than the dual-frequency PPP except for the IF-PPP2 model. Consequently, we can conclude that the PPP performances in terms of positioning accuracy and reliability can be improved with the multi-GNSS combination and more available frequency signals in kinematic scenarios.

4. Conclusion

This paper assessed and analyzed the performances of multi-frequency PPP models for GPS, BeiDou, GLONASS, Galileo and QZSS. In total, four multi-frequency PPP mathematical models, named IF-PPP1, IF-PPP2, UC-PPP and IC-PPP, were developed, as well as their stochastic models. These models also apply for single-, dual-, triple-, quad- and five-constellation GNSS data processing.

First, static datasets collected at 18 MGEX stations over 30 consecutive days were utilized to evaluate the multi-frequency PPP models. The dual-frequency IF PPP, namely IF-PPP0, was also tested for comparison. Comparative analysis shows that the BeiDou-only and Galileo-only PPP perform worse than the GPS-only solution and the multi-GNSS integration can significantly improve the multi-frequency PPP performances. The performances of triple-frequency PPP generally agree well with each other and the triple-frequency PPP models perform slightly better than the dual-frequency

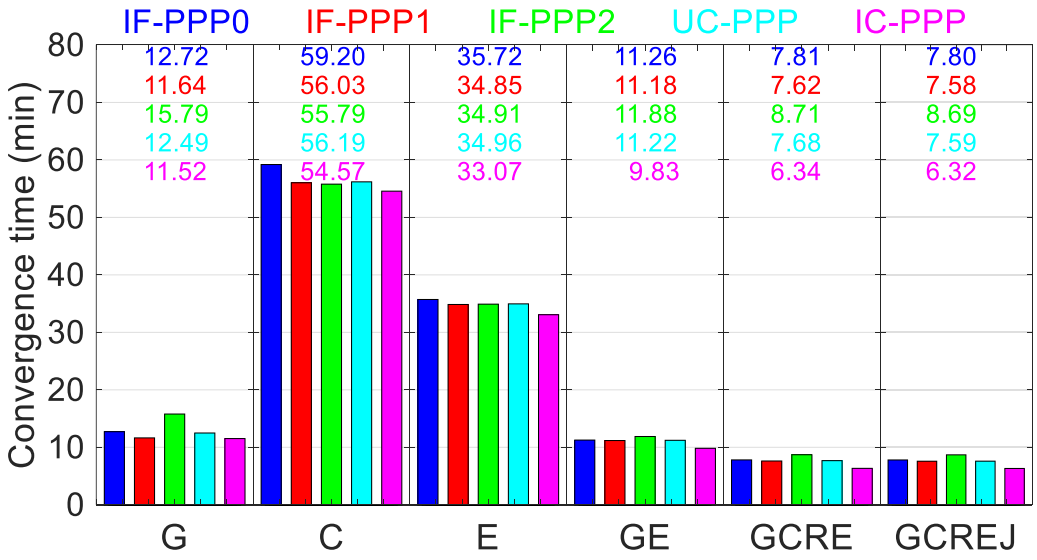

Figure 8. Mean convergence times of 18 stations by different PPP models for GPS-only, BeiDou-only, Galileo-only, GPS/Galileo, GPS/BeiDou/GLONASS/Galileo and five-constellation solutions.

Table 4. RMS errors of 18 stations by different PPP models for GPS-only, BeiDou-only, Galileo-only, GPS/Galileo, GPS/BeiDou/GLONASS/Galileo and five-constellation solutions (unit: mm).

Type	RMS	IF-PPP0	IF-PPP1	IF-PPP2	UC-PPP	IC-PPP
G	N	5.30	5.16	7.65	5.13	5.20
G	E	11.60	11.42	16.50	11.43	11.41
G	U	15.91	15.21	18.95	15.25	15.34
C	N	11.04	11.05	11.06	11.11	12.93
C	E	16.68	16.75	16.40	16.57	17.50
C	U	50.59	50.43	50.51	50.48	48.72
E	N	7.88	7.86	7.87	7.85	7.95
E	E	11.84	11.81	11.85	11.89	12.11
E	U	23.96	23.90	23.81	23.90	23.11
GE	N	4.86	4.81	6.10	4.81	4.78
GE	E	10.17	9.86	12.27	9.89	9.86
GE	U	14.52	14.34	17.99	14.44	14.22
GCRE	N	4.75	4.54	5.04	4.55	4.51
GCRE	E	9.04	9.32	9.20	9.30	9.27
GCRE	U	13.38	13.19	15.54	13.23	13.14
GCREJ	N	4.75	4.53	5.04	4.55	4.49
GCREJ	E	9.03	9.32	9.21	9.29	9.28
GCREJ	U	13.38	13.18	15.52	13.23	13.12

solution, except for the GPS under the IF-PPP2 model. By introducing GIM products, the mean convergence time of the multi-frequency PPP model is reduced. Compared with the IF-PPP0 model, the mean convergence time of the IC-PPP is reduced by 7.4% from 35.7 to 33.1 min and by 19.0% from 7.8 to 6.3 min for the Galileo-only and five-constellation IC-PPP, respectively. In addition, the estimated receiver clocks, ZTDs, IFBs and DCBs were also evaluated. Finally, a vehicle-borne experiment was used to test the PPP performances in kinematic scenarios, the performances of which can be improved with more frequency signals and GNSS observations.

The BeiDou multi-frequency PPP performances can be improved since the BeiDou-3 satellites have officially

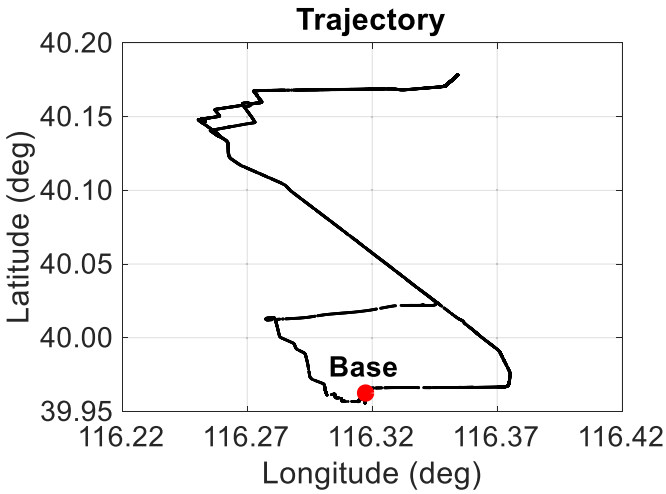

Figure 9. Trajectory of the vehicle-borne experiment.

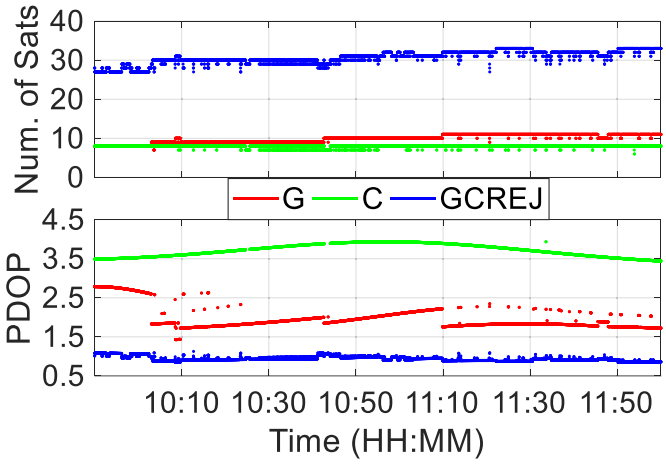

Figure 10. Number of satellites and PDOP of the vehicle-borne kinematic data (DOY 89, 2018).

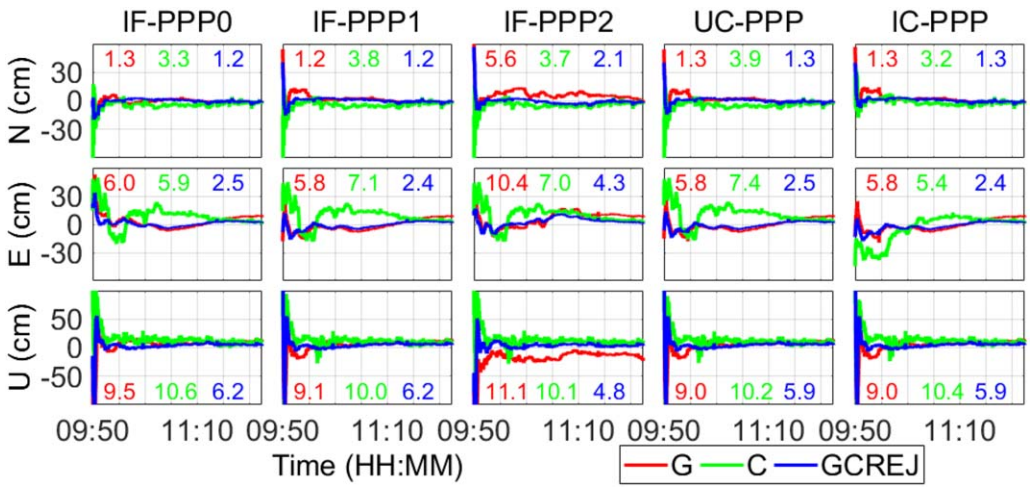

Figure 11. Kinematic positioning errors of the multi-frequency PPP models for the vehicle-borne kinematic data (DOY 89, 2018).

provided global services since December 2018. We acknowledge that only BeiDou-2 PPP solutions for BeiDou are considered in this study. Investigations on BeiDou-3 multi-frequency PPP will be conducted in the future.

Acknowledgments

This research is supported by the National Natural Science Foundation of China German Science Foundation (NSFC-DFG) Project (Grant No. 41761134092). The authors gratefully acknowledge the GFZ for providing products and IGS for the datasets.

ORCID iDs

Ke Su https://orcid.org/0000-0003-3039-5106
Shuanggen Jin https://orcid.org/0000-0002-5108-4828
Guoqiang Jiao https://orcid.org/0000-0003-3768-5341

References

[1] Li X, Li X, Liu G, Feng G, Yuan Y, Zhang K and Ren X 2019 Triple-frequency PPP ambiguity resolution with multi-constellation GNSS: BDS and Galileo *J. Geod.* **93** 1105–122
[2] Montenbruck O, Hugentobler U, Dach R, Steigenberger P and Hauschild A 2012 Apparent clock variations of the Block IIF-1 (SVN62) GPS satellite *GPS Solut.* **16** 303–13
[3] Yang Y X, Li J, Xu J, Tang J, Guo H and He H 2011 Contribution of the compass satellite navigation system to global PNT users *Sci. Bull.* **56** 2813–9
[4] Montenbruck O, Hauschild A, Steigenberger P, Hugentobler U, Teunissen P and Nakamura S 2013 Initial assessment of the COMPASS/BeiDou-2 regional navigation satellite system *GPS Solut.* **17** 211–22
[5] Xiao W, Liu W and Sun G 2016 Modernization milestone: BeiDou M2-S initial signal analysis *GPS Solut.* **20** 125–33
[6] Zaminpardaz S, Teunissen P J G and Nadarajah N 2017 GLONASS CDMA L3 ambiguity resolution and positioning *GPS Solut.* **21** 535–49
[7] Tu R, Liu J, Zhang R, Zhang P, Huang X and Lu X 2019 RTK model and positioning performance analysis using Galileo four-frequency observations *Adv. Space Res.* **63** 913–26
[8] Wang K, Chen P, Zaminpardaz S and Teunissen P J G 2019 Precise regional L5 positioning with IRNSS and QZSS: stand-alone and combined *GPS Solut.* **23** 10
[9] Zhang X and He X 2016 Performance analysis of triple-frequency ambiguity resolution with BeiDou observations *GPS Solut.* **20** 269–81
[10] Gu S, Lou Y, Shi C and Liu J 2015 BeiDou phase bias estimation and its application in precise point positioning with triple-frequency observable *J. Geod.* **89** 979–92
[11] Zhao D, Roberts G W, Hancock C M, Lau L and Bai R 2019 A triple-frequency cycle slip detection and correction method based on modified HMW combinations applied on GPS and BDS *GPS Solut.* **23** 22
[12] Li X, Ge M, Dai X, Ren X, Fritsche M, Wickert J and Schuh H 2015 Accuracy and reliability of multi-GNSS real-time precise positioning: GPS, GLONASS, BeiDou, and Galileo *J. Geod.* **89** 607–35
[13] Tu R, Liu J, Zhang R, Fan L, Zhang P and Han J 2019 Real-time kinematic positioning algorithm with GNSS and high-frequency accelerometer observations for broadband signals *Meas. Sci. Technol.* **31** 035007
[14] Vollath U, Birnbach S, Landau L, Fraile-Ordoñez J M and Martí-Neira M 1999 Analysis of three-carrier ambiguity resolution technique for precise relative positioning in GNSS-2 *Navigation* **46** 13–23
[15] Hatch R, Jung J, Enge P and Pervan B 2000 Civilian GPS: the benefits of three frequencies *GPS Solut.* **3** 1–9
[16] Li B, Feng Y, Gao W and Li Z 2015 Real-time kinematic positioning over long baselines using triple-frequency BeiDou signals *IEEE Trans. Aerosp. Electron. Syst.* **51** 3254–69
[17] Geng J and Bock Y 2013 Triple-frequency GPS precise point positioning with rapid ambiguity resolution *J. Geod.* **87** 449–60
[18] Tegedor J and Øvstedal O 2014 Triple carrier precise point positioning (PPP) using GPS L5 *Surv. Rev.* **46** 288–97
[19] Guo F and Zhang X 2016 Modeling and assessment of triple-frequency BDS precise point positioning *J. Geod.* **90** 1223–35
[20] Tu R, Zhang P, Zhang R, Liu J and Lu X 2018 Modeling and performance analysis of precise time transfer based on BDS triple-frequency un-combined observations *J. Geod.* **93** 837–47
[21] Pan L, Zhang X, Li X, Liu J and Xin L 2017 Characteristics of inter-frequency clock bias for Block IIF satellites and its

effect on triple-frequency GPS precise point positioning *GPS Solut.* **21** 811–22
[22] Zhao L, Ye S and Song J 2017 Handling the satellite inter-frequency biases in triple-frequency observations *Adv. Space Res.* **59** 2048–57
[23] Leick A, Rapoport L and Tatarnikov D 2015 *GPS Satellite Surveying* (New York: Wiley)
[24] Guo F, Zhang X and Wang J 2015 Timing group delay and differential code bias corrections for BeiDou positioning *J. Geod.* **89** 427–45
[25] Su K and Jin S 2019 Triple-frequency carrier phase precise time and frequency transfer models for BDS-3 *GPS Solut.* **23** 86
[26] Tu R, Zhang P, Zhang R, Liu J and Lu X 2018 Modeling and assessment of precise time transfer by using BeiDou navigation satellite system triple-frequency signals *Sensors* **18** 1017
[27] Li X, Liu G, Li X, Zhou F, Feng G, Yuan Y and Zhang K 2020 Galileo PPP rapid ambiguity resolution with five-frequency observations *GPS Solut.* **24** 24
[28] El-Mowafy A, Deo M and Rizos C 2016 On biases in precise point positioning with multi-constellation and multi-frequency GNSS data *Meas. Sci. Technol.* **27** 035102
[29] Tu R, Zhang R, Zhang P, Liu J and Lu X 2018 An approach for real-time fast point positioning of the BeiDou navigation satellite system using augmentation information *Meas. Sci. Technol.* **29** 075003
[30] Su K, Jin S and Hoque M 2019 Evaluation of ionospheric delay effects on multi-GNSS positioning performance *Remote Sens.* **11** 171
[31] Guo F, Li X, Zhang X and Wang J 2017 Assessment of precise orbit and clock products for Galileo, BeiDou, and QZSS from IGS Multi-GNSS Experiment (MGEX) *GPS Solut.* **21** 279–90
[32] Wang N, Yuan Y, Li Z, Montenbruck O and Tan B 2016 Determination of differential code biases with multi-GNSS observations *J. Geod.* **90** 209–28
[33] Tu R, Hong J, Zhang R, Han J, Fan L, Zhang P, Liu J and Lu X 2019 GPS and BDS combined PPP model with inter-system differenced observations *Adv. Space Res.* **65** 494–505
[34] Steigenberger P, Hauschild A, Montenbruck O, Rodriguez-Solano C and Hugentobler U 2013 Orbit and clock determination of QZS-1 based on the CONGO network *Navigation* **60** 31–40
[35] Cao X, Li J, Zhang S, Kuang K, Gao K, Zhao Q and Hong H 2018 Uncombined precise point positioning with triple-frequency GNSS signals *Adv. Space Res.* **63** 2745–56
[36] Su K and Jin S 2018 Improvement of multi-GNSS precise point positioning performances with real meteorological data *J. Navig.* **71** 1363–80
[37] Kouba J 2009 A guide to using International GNSS Service (IGS) products (http://igscb.jpl.nasa.gov/igscb/resource/pubs/UsingIGSProductsVer21.pdf)
[38] Petit G and Luzum B 2010 *IERS conventions (2010) (No. IERS-TN-36)* (France: Bureau International Des Poids et Mesures Sevres)
[39] Wu J-T, Wu S C, Hajj G A, Bertiger W I and Lichten S M 1991 Effects of antenna orientation on GPS carrier phase[C] *Astrodynamics* **1992** 1647–60
[40] Xu G and Xu Y 2016 *GPS: theory, algorithms and applications[M]* (Berlin: Springer)
[41] Byun S H and Bar-Sever Y E 2009 A new type of troposphere zenith path delay product of the international GNSS service *J. Geod.* **83** 1–7
[42] Su K, Jin S and Ge Y 2019 Rapid displacement determination with a stand-alone multi-GNSS receiver: GPS BeiDou, GLONASS, and Galileo *GPS Solut.* **23** 54